Electronic Supplementary Material (ESI) for Lab on a Chip.

Portable all-in-one microfluidic system for CRISPR–Cas13a-based fully integrated multiplexed nucleic acid detection

Ya Zhang, ‡[ab] Yue Guo, ‡[cd] Guozhen Liu,[ab] Shiqi Zhou,[ab] Rouyu Su,[ab] Qian Ma,[ab] Yiyue Ge,[cd] Yan-qing Lu,*[a] Lunbiao Cui*[cd] and Guanghui Wang*[ab]

a. College of Engineering and Applied Sciences, Nanjing University, Jiangsu 210093, China.
b. Key Laboratory of Intelligent Optical Sensing and Integration of the Ministry of Education, Nanjing University, Jiangsu 210009, China.
c. NHC Key Laboratory of Enteric Pathogenic Microbiology, Jiangsu Provincial Medical Key Laboratory of Pathogenic Microbiology in Emerging Major Infectious Diseases, Jiangsu 210009, China.
d. Jiangsu Province Engineering Research Center of Health Emergency, Jiangsu Provincial Center for Disease Control and Prevention, Jiangsu 210009, China.
‡ These authors contributed equally to this paper.

Email: yqlu@nju.edu.cn (Y.L.), lbcui@jscdc.cn (L.C.), wangguanghui@nju.edu.cn(G.W.).

Materials and Methods

1. Reagents and materials

1.1 Design of primers and probes

This study focused on the pathogens of severe infectious diseases that have occurred in recent years, including Japanese encephalitis virus (JEV), yellow fever virus (YEV), West Nile virus (WNV), Ebola virus (EBOV), Chikungunya virus (CHIKV), Crimean-Congo haemorrhagic fever virus (CCHFV), dengue virus (DENV), Rift Valley fever virus (RVFV), Zika virus (ZIKV) and Marburg virus (MARV). To design primers for the templates, the complete genome sequences from the National Center for Biotechnology Information were aligned and analysed. The primers were designed to target highly conserved regions of the templates. The primers were designed using Lasergene™ (DNASTAR, Madison, WI, USA). The specificity of the sequences of the selected primers and probes was verified by a basic local alignment search tool (BLAST) search in the nucleotide database of GenBank. To design RAA-specific primers, we added the T7 promoter sequence 5'-TAATACGACTCACTATAGGG-3' to the 5'-end of the forward primer. The reverse complement of the T7 promoter sequence and the detection probe sequence was added to the 3'-end of the crRNA sequence. Table S1 shows the sequences of the primers and probes.

1.2 crRNA design and preparation

The single-stranded DNA (ssDNA) template for in vitro transcription was synthesized by Sangon Biotech Inc. (China). First, the transcription template was incubated with 5 μL of T7 RNA polymerase buffer, 1 μL of T7 promoter, 5 μL of DTT (50 mmol/L), 4 μL of NTP mix (25 mmol/L), 1.25 μL of recombinant RNase inhibitor and 2.5 μL of T7 RNA polymerase at 42 °C for 2 h to prepare crRNA. Then, the product was incubated with 2 μL of recombinant DNase I (RNase-free) at 37 °C for 1 h. Finally, sgRNA was purified by a Spin Column RNA Cleanup & Concentration Kit (Sangon Biotech Inc., China). All crRNA sequences are listed in Table S1.

1.3 Preparation of the dsDNA targets

The pUC57-dsDNA plasmid containing the targets for the infectious disease pathogens was provided by Sangon Biotech Inc. (China). E. coli competent cells were transformed with the pUC57-dsDNA plasmid. The transformed E. coli strain was added to 15% glycerin (final concentration) and stored at −80 °C. The transformed E. coli strain was cultured in LB medium (10 g/L tryptone, 5 g/L yeast extract, 10 g/L NaCl) containing 50 μg/mL ampicillin at 37 °C for 16 h. The bacterial solution was extracted with a MiniBEST Plasmid Purification Kit (TaKaRa

Biotechnology, Kusatsu, Japan). The plasmids were quantified with a Qubit™ dsDNA BR Assay Kit (Thermo Fisher Scientific, US) after sequencing verification.

1.4 MB-based nucleic acid (NA) extraction

A GenMag™ Viral DNA/RNA extraction kit was used to purify RNA from plasma samples. The reagent storage module of the chip was preloaded with 300 μL lysis buffer, 300 μL Wash Buffer I, 300 μL Wash Buffer II, 300 μL Wash Buffer III and elution buffer. Ten microlitres of proteinase K, 4 μL of acryl carrier and 20 μL of MBs were lyophilized into the NA extraction reaction chamber.

1.5 Recombinase-assisted amplification (RAA)

The RAA kit was from Jiangsu Qitian Biotechnology. The 25 μL buffer and 2.5 μL magnesium acetate were mixed and preloaded into the reagent storage module of the chip. A mixture of 2 μL of 10 μmol/L forward primer, 2 μL of 10 μmol/L reverse primer, enzymes, polyethylene glycol 20,000 (0.1%, Sigma-Aldrich), and trehalose [10% (w/v), Sigma-Aldrich] needed for the reaction were lyophilized into the RAA reaction chamber. After reagent freeze-drying and packaging, the final chip can be stored at room temperature for one month. In an un-freeze-drying process, the detection performance of the chip decreased rapidly within one week (Figure S12).

1.6 CRISPR–Cas13a system

A mixture of 1 μL of 25 mmol/L NTP (Thermo Fisher Scientific, US), 20 U of recombinant RNase inhibitor (TaKaRa Biotechnology, Kusatsu, Japan), 15 U of T7 RNA polymerase (TaKaRa Biotechnology, Kusatsu, Japan), 1 μL of 20 μmol/L RNA probe, 3 μL of Cas13a (Gene universal technology Co. Ltd., China) and 1.4 μL Cr RNA were lyophilized into the detection chamber. Five microlitres of 5× HEPES buffer (20 mmol/L Heps [TaKaRa Biotechnology, Kusatsu, Japan], 60 mmol/L NaCl, 6 mmol/L $MgCl_2$, pH 6.8) and 10.8 μL RNase free water (TaKaRa Biotechnology, Kusatsu, Japan) were mixed and preloaded into the reagent storage module of the chip.

Further details on primers, probes and Cr RNA sequences can be found in table S1.

2. 3D printing structure

The shell and the internal structure are designed in SolidWorks 2019 and fabricated via a 3D printing service provider (WeNext Co., Ltd., Shenzhen, China). The shell of the device was printed with white resin material with a resolution of 200 μm. To block the ambient light

and the fluorescence of the substrate material, the optical module uses a black high-performance nylon material (HP3DHR-PA12) with a resolution of 200 μm.

3. Hardware system design

Figure S1 shows the logical relationship between those main components in the total equipment. For users, they only need to select operational procedure file and then click the start button. Next, the system will automatically execute each instruction one by one and control all the connected components in a wired or wireless manner, ultimately achieving the user's needs.

First, the main control PCB is linked with the high precision motor (323890, Maxon, Switzerland) through the servo controller, which can provide precise control of the speed, acceleration and angle position, with a nominal speed of 6990 rpm and position accuracy of 0.18 degrees. After the weight distribution optimization for the rotating functional box, the maximum allowed rotating speed with loading is 3000 rpm. Second, the main control PCB is also connected with a pair of power coupling coils, which provide a stable power supply for the rotating functional box above them. Third, the rotating functional box communicates with the main control PCB in a wireless manner using the ZigBee protocol. In this way, the system can control the wax valve and the magnetic switching structure while they are rotating with the chip. Next, a ring rubber heater and three thermistors are used for the temperature control of the air chamber. Then, there are four fluorescent detection modules (FAM, HEX, ROX, CY5) are installed on the motor-driven rising detection box. The fluorescence signal collected by a photodetector is transmitted to the main control board through a universal asynchronous receiver/transmitter (UART) and displayed on the screen of the device in real time. Finally, an LCD screen is used for the UI interface and result display.

The rotating functional box consists of the following modules (Figure S2):

The stationary wireless power transmitter coil is fixed on the platform underneath the functional box, while the upper receiver coil and the power coupling PCB are fixed at the bottom of the rotating functional box and rotate with it. It rectifies and filters the alternating current (AC) power from the coil and generates a stable voltage of 5 V to the upper layers. The output voltage ranges from 5.00 V to 5.40 V, with a peak to peak value of 400 mV. The second layer is the CPU and ZigBee PCB, which is the control unit of the rotating functional box with an ARM microcontroller system. It controls the magnetic switching structure and performs the switching between the magnetic and nonmagnetic states. It also controls the MCH and open the

paraffin wax valves for flow control. Moreover, it also wirelessly communicates with the stationary main control PCB by using ZigBee protocol. The third layer is the contact pin array PCB thimble board, which supplies power to the valve heating PCB above the rotating subassemblies. The fourth layer is the valve heating PCB with MCH. It can quickly heat up and melt the paraffin wax block and open the valve in the chip layer. The heating of each MCH and the opening of the paraffin wax valve can be independently controlled. The different paraffin wax valves do not interfere with each other and can be arranged in a high density on the chip. The top layer is a microfluidic chip with localized wax valves, enabling the orderly release of reagents with the aid of the paraffin wax valves.

4. Magnetic switching structure

The magnetic switching structure consists of the bidirectional self-retaining electromagnet (BS-0521 N-33, Boshun, Dongguan), a connecting rod, a placement plate for the magnet and the square Nd-Fe-B permanent magnet. The maximum pushing or pulling force of the electromagnet can reach 140 g. The size of the Nd-Fe-B permanent magnet is 15×8×4 mm (N35). These magnets are installed in a 3D-printed plate. The distance from the magnet to chip is 2.6 mm. When the bidirectional self-retaining electromagnet receives the reverse voltage signal, the connecting rod is pushed to cause the placement plate to rotate. At this time, the Nd-Fe-B permanent magnet is located directly below the sample chamber, and the magnetic field strength is 32.15 mT. The magnetic beads in the sample chamber are completely adsorbed on the bottom surface of the chamber. When a nonmagnetic state is needed, the bidirectional self-retaining electromagnet receives the forward voltage signal and pulls back the placement plate through the connecting rod. At this time, the sample chamber is staggered with the Nd-Fe-B permanent magnet at an angle of 32.81°. The magnetic field strength is greatly weakened to 0.59 mT; thus, the magnet force is too weak to act on the sample chamber.

5. Design scheme of the optical path and structure

The optimal parameters, such as excitation beam diameter DL, distance from the objective lens to detection plane L1, and diameter of microfluidic chip detection chamber dF, were determined via ZEMAX simulation and optimization. Based on the optimization, the focal length of the lens is 12 mm, the distance between the objective lens and eyepiece is 18 mm, and the distance between the receiving surface of the photodetector and eyepiece is 3.5 mm. The excited fluorescence is converged by a lens to illuminate the photosensitive surface of the

photodetector with a circular focusing spot with a field of view r = 0.5 mm after passing through the dichroscope and filter.

Figure S4D shows the hardware system framework of the fluorescence detection module and circuit board. A microcontroller unit (MCU) mainly attains the acquisition of the analogue signal and digital signal of the fluorescence detection module and outputs the control signal at the same time to provide closed-loop control. The fluorescence detection module transmits the numerical signal of the fluorescence intensity to the main control PCB through the universal asynchronous receiver/transmitter (UART), and the entire detection process is completed. The fluorescence detection module laser is regulated by the duty cycle of pulse width modulation (PWM) and its stability is assisted by temperature regulation. The system compensates according to the semiconductor laser temperature collected by the negative temperature coefficient (NTC) thermistor. When the semiconductor laser temperature is higher than the set value, the microprocessor controls opening the semiconductor refrigeration chip for heat dissipation, and when the temperature is lower than the set temperature, the microprocessor controls closing the semiconductor refrigeration chip. After adjusting the temperature of the semiconductor laser, the power of the semiconductor laser can be stabilized at the set value (Figure S4E and S4F).

6. Chip design

Our complex chip consists of a permanent PCB layer and a disposable microchannel disc (including an upper chip cover, a microchannel layer and a bottom chip cover), which can be assembled and disassembled by buckles. The centrifugal disc comprises the main structure of PC and two sealing membranes, which are sealed by double-sided adhesive tape (467MP, 3M). The assembled chip is in electrical contact with the rotating functional box by using a spring-loaded pin array. With the power controlled by the rotating functional box, we can introduce the separately controllable thermally activated paraffin wax valves. The design of the wax valve is shown in Figure S5. It has a vertical hole on the top surface for wax injection. Its chamber is located at the bottom of the microchannel layer for a better heating effect. The chamber is covered by a PC layer of 0.3 mm thickness. The volume of injected wax to fill the chamber is only approximately 1.2 μL. Beneath each valve, there is a corresponding heating element on the PCB layer (Figure S6C and S6D). Since the corresponding heater is very close, it can quickly melt the wax block in 2 s. During the disc rotation, the melting wax leaves the heating region, opening the valve. Furthermore, the heating is also very localized, and the valves

on PCBs can be activated separately, as long as their interval is larger than 5 mm, thus ensuring the high-density integration of the valves.

7. Melting wax auto dispensing system

To form wax valves within the chip efficiently and accurately, we set up a melting wax automatic dispensing system (Figure S7). The system includes an air compression pump and its pressure controller and a dispensing syringe tube and its temperature controller. Furthermore, an additional temperature controller is also needed for the syringe needle since the paraffin wax can solidify and block the needle. Approximately 15 g of solid paraffin wax particles with a melting point of 48 °C is filled into the syringe tube. The temperature of the syringe tube is set at 65 °C, while that of the syringe needle is set at 60 °C. The syringe needle is inserted into the top hole, and the control button trigger is pressed to open the pressure within a small time slot. By adjusting the time duration and pressure value, we can accurately control the volume of ejected liquid wax. For volumes of 1 μL and 2 μL with 0.1 Psi, the time duration is approximately 0.1 s and 0.2 s, respectively. A video of the melting wax auto dispensing system is provided in Supporting movie 4.

8. Air heating unit for temperature control

A ring heating rubber and three negative temperature coefficient (NTC) thermistors for temperature sampling are placed in the air chamber, and the PID algorithm is used to achieve temperature control with a temperature accuracy of ±0.5 °C (Figure S13). In addition, the spinning of the chip also ensures the uniformity of the temperature inside the chamber. Due to the poor thermal conductivity of polycarbonate (PC), the air temperature needs to be slightly higher than the target value, which is approximately 2.5 °C, based on the in-chip calibration.

9. Operational procedure file

InitialHeatingParameters,1,2,3,4,5,6,7,9,10,11,12,13,14,15,17,18,19,20,21,22,23,24,25,26,27,28,29,30,31,32,33,34,35,36,37,38,39,40

DetResArray=zeros(PositionNo, SamplingNo, loopCount);

RefResArray=zeros(2, SamplingNo, loopCount);

Parameter Setting:

OpenValveSpeed 400;

OpenValveT 2;

RefDetPos 100;

PositionNo 7;

PositionArray [200;350;500;800;1200;1800;1998];

DetIntTime 100;

SamplingNo 100;

loopCount 100;

loopIntevalTime 10000;

LaserNo 1;

EnvTem 3900;

1) Open paraffin wax valve 1/1' and 2/2' (Lysis buffer), Heating for 2 seconds

OpenValve, 2, 2

OpenValve, 5, 2

OpenValve, 37, 2

OpenValve, 39, 2

 # Start rotating at 400 rpm, Acceleration of 200 rpm/s, lasting 5 s

SetMotorVelocityAndRunTime, 0, 400, 200, 5

 # 800 rpm for each clockwise and counterclockwise rotation, acceleration of 800 rpm/s, 300 cycles

SwingDisk, 300, 800, 800

 # Switching to magnetic state

SwitchOnMagnetic

 # Start rotating after 10 s

Delay, 10000

 # Start rotating at 800 rpm, Acceleration of 200 rpm/s, lasting 10 s

SetMotorVelocityAndRunTime, 0, 800, 200, 10

 # Switching to no-magnetic state

SwitchOffMagnetic

2) Open paraffin wax valve 3/3' (Wash buffer I), Heating for 2 seconds

OpenValve, 11, 2

OpenValve, 24, 2

 # Start rotating at 400 rpm, Acceleration of 200 rpm/s, lasting 5 s

SetMotorVelocityAndRunTime, 0, 400, 200, 5

 # 800 rpm for each clockwise and counterclockwise rotation, acceleration of 800 rpm/s, 30 cycles

SwingDisk, 30, 800, 800

 # Switching to magnetic state

SwitchOnMagnetic

 # Start rotating after 10 s

Delay, 10000

 # Start rotating at 800 rpm, Acceleration of 200 rpm/s, lasting 10 s

SetMotorVelocityAndRunTime, 0, 800, 200, 10

 # Switching to no-magnetic state

SwitchOffMagnetic

3) Open paraffin wax valve 4/4’ (Wash buffer II), Heating for 2 seconds

OpenValve, 12, 2

OpenValve, 23, 2

 # Start rotating at 400 rpm, Acceleration of 200 rpm/s, lasting 5 s

SetMotorVelocityAndRunTime, 0, 400, 200, 5

 # 800 rpm for each clockwise and counterclockwise rotation, acceleration of 800 rpm/s, 30 cycles

SwingDisk, 30, 800, 800

 # Switching to magnetic state

SwitchOnMagnetic

 # Start rotating after 10 s

Delay, 10000

 # Start rotating at 800 rpm, Acceleration of 200 rpm/s, lasting 10 s

SetMotorVelocityAndRunTime, 0, 800, 200, 10

4) Open paraffin wax valve 5/5’ (Wash buffer III), Heating for 2 seconds

OpenValve, 15, 2

OpenValve, 22, 2

 # Start rotating at 400 rpm, Acceleration of 200 rpm/s, lasting 5 s

SetMotorVelocityAndRunTime, 0, 400, 200, 5

 # Start rotating after 10 s

Delay, 10000

 # Start rotating at 800 rpm, Acceleration of 200 rpm/s, lasting 10 s

SetMotorVelocityAndRunTime, 0, 800, 200, 10

5) Open paraffin wax valve 6/6’ (Elution buffer), Heating for 2 seconds

OpenValve, 20, 2

OpenValve, 21, 2

 # Start rotating at 400 rpm, Acceleration of 200 rpm/s, lasting 5 s

SetMotorVelocityAndRunTime, 0, 400, 200, 5

 # 800 rpm for each clockwise and counter clockwise rotation, acceleration of 800 rpm/s, 150 cycles

SwingDisk, 150, 800, 800

 # Switching to magnetic state

SwitchOnMagnetic

 # Start rotating after 10 s

Delay, 10000

6) Open paraffin wax valve 8/8’ (reaction chamber), Heating for 2 seconds

OpenValve, 38, 2

OpenValve, 40, 2

 # Start rotating at 700 rpm, Acceleration of 200 rpm/s, lasting 10 s

SetMotorVelocityAndRunTime, 0, 700, 200, 10

 # Start rotating at 1000 rpm, Acceleration of 500 rpm/s, lasting 10 s

SetMotorVelocityAndRunTime, 0, 1000, 500, 10

7) Open paraffin wax valve 7/7’ (RAA buffer), Heating for 2 seconds

OpenValve, 36, 2

OpenValve, 10, 2

 # Start rotating at 700 rpm, Acceleration of 200 rpm/s, lasting 10 s

SetMotorVelocityAndRunTime, 0, 700, 200, 20

 # Start rotating at 1000 rpm, Acceleration of 500 rpm/s, lasting 10 s

SetMotorVelocityAndRunTime, 0, 1000, 500, 10

8) Heat to 39°C. P=0.005, I=0.001, D=0.0005

SetTargetTemperature, EnvTem, 0.005, 0.001, 0.0005

 # Temperature data is collected every 5 s for graphing

StartLogTemperature,5

 # Stop collecting temperature data after 1200 s

Delay,1200000

StopLogTemperature

9) Open paraffin wax valve 10/10' (RAA product), Heating for 2 seconds

OpenValve, 25, 2

OpenValve, 26, 2

OpenValve, 27, 2

OpenValve, 28, 2

OpenValve, 29, 2

OpenValve, 30, 2

OpenValve, 31, 2

OpenValve, 32, 2

OpenValve, 33, 2

OpenValve, 34, 2

OpenValve, 3, 2

OpenValve, 4, 2

OpenValve, 6, 2

OpenValve, 7, 2

OpenValve, 9, 2

OpenValve, 13, 2

OpenValve, 14, 2

OpenValve, 17, 2

OpenValve, 18, 2

OpenValve, 19, 2

 # Start rotating at 700 rpm, Acceleration of 200 rpm/s, lasting 5 s

SetMotorVelocityAndRunTime, 0, 700, 200, 5

 # Start rotating at 1000 rpm, Acceleration of 500 rpm/s, lasting 10 s

SetMotorVelocityAndRunTime, 0, 1000, 500, 10

10) Open paraffin wax valve 9/9’ (CRISPR buffer), Heating for 2 seconds

OpenValve, 35, 2

OpenValve, 1, 2

 # Start rotating at 700 rpm, Acceleration of 200 rpm/s, lasting 5 s

SetMotorVelocityAndRunTime, 0, 700, 200, 5

 # Start rotating at 1000 rpm, Acceleration of 500 rpm/s, lasting 10 s

SetMotorVelocityAndRunTime, 0, 1000, 500, 10

11) Heat to 39°C. P=0.005, I=0.001, D=0.0005

SetTargetTemperature, EnvTem, 0.005, 0.001, 0.0005

 # Temperature data is collected every 5 s for graphing

StartLogTemperature,5

 # Stop collecting temperature data after 900 s

Delay,900000

StopLogTemperature

 # Turn on laser 1 and set the power to 10 mW.

 # The frequency of the PWM regulation signal is 1000 Hz and the duty cycle is 20 %.

OpenLaser, 1, 20, 1000, 20

RunOpticalDetect, 200, 30, 12, 150, 300, 200, 1000, 0

CloseLaser

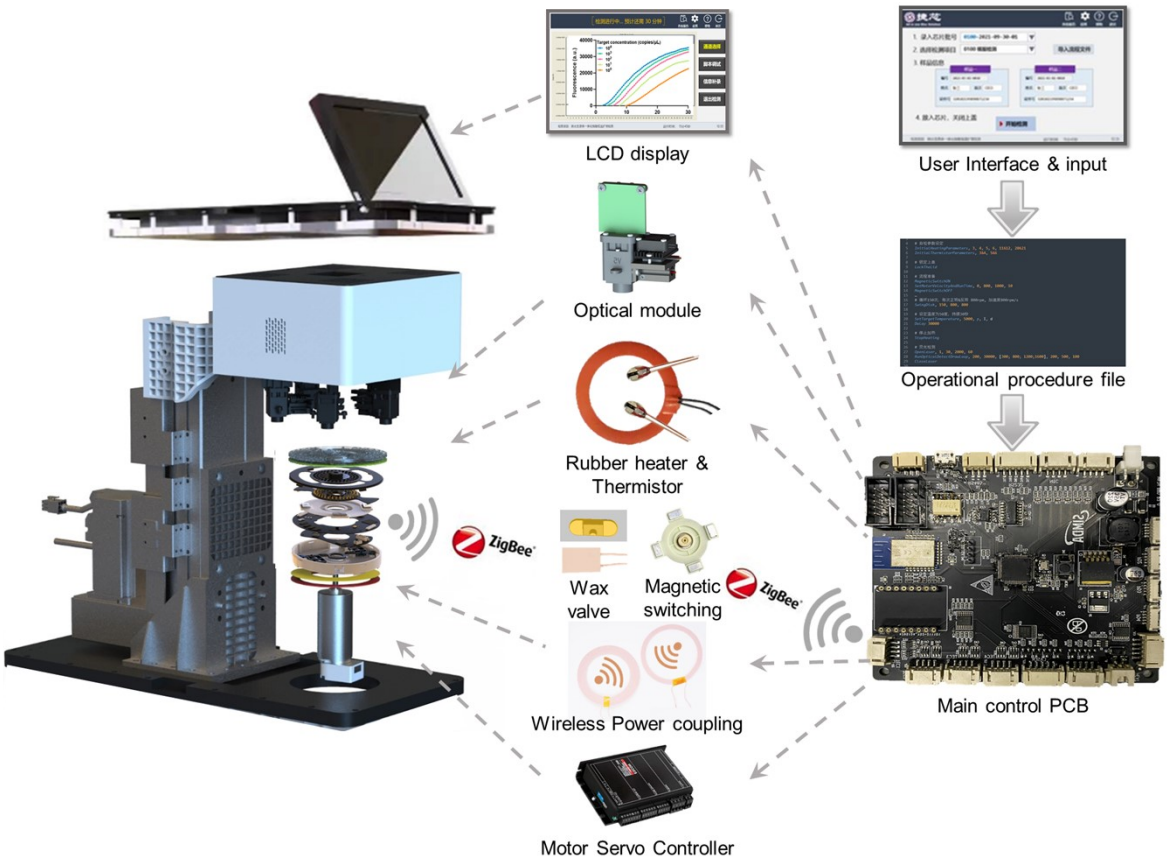

Figure S1. Workflow of the hardware system.

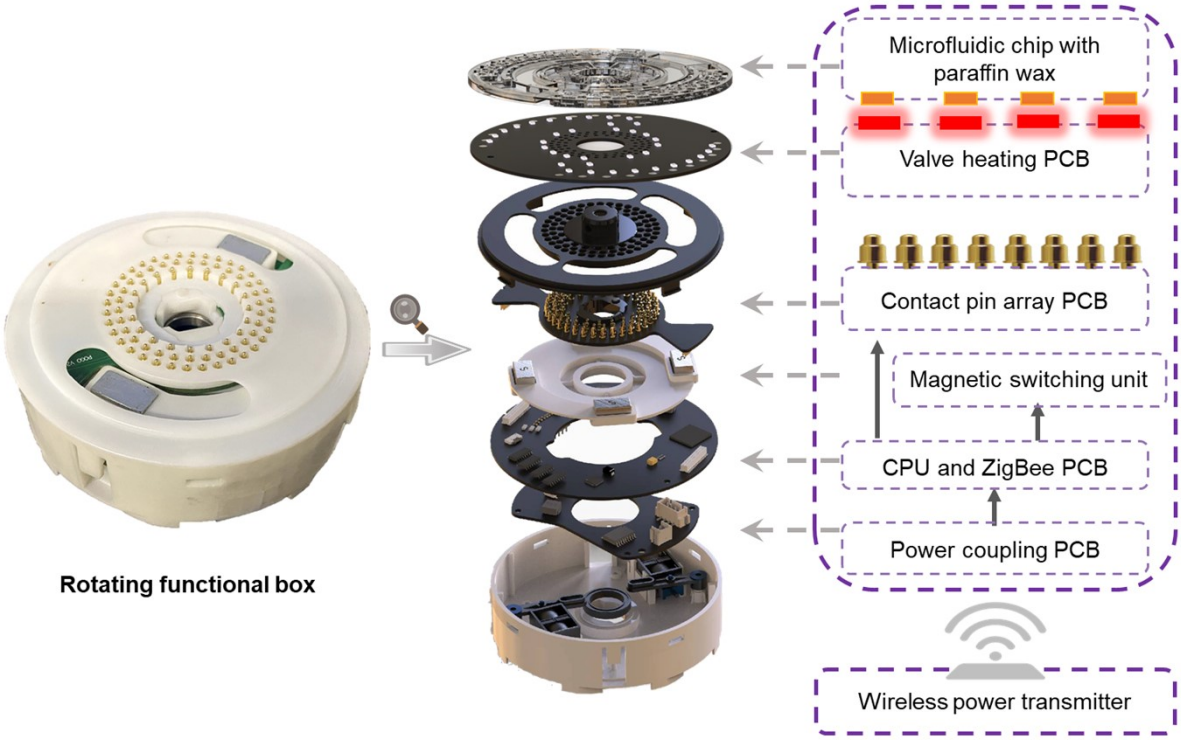

Figure S2. Design layout and schematic diagram of the rotating functional box.

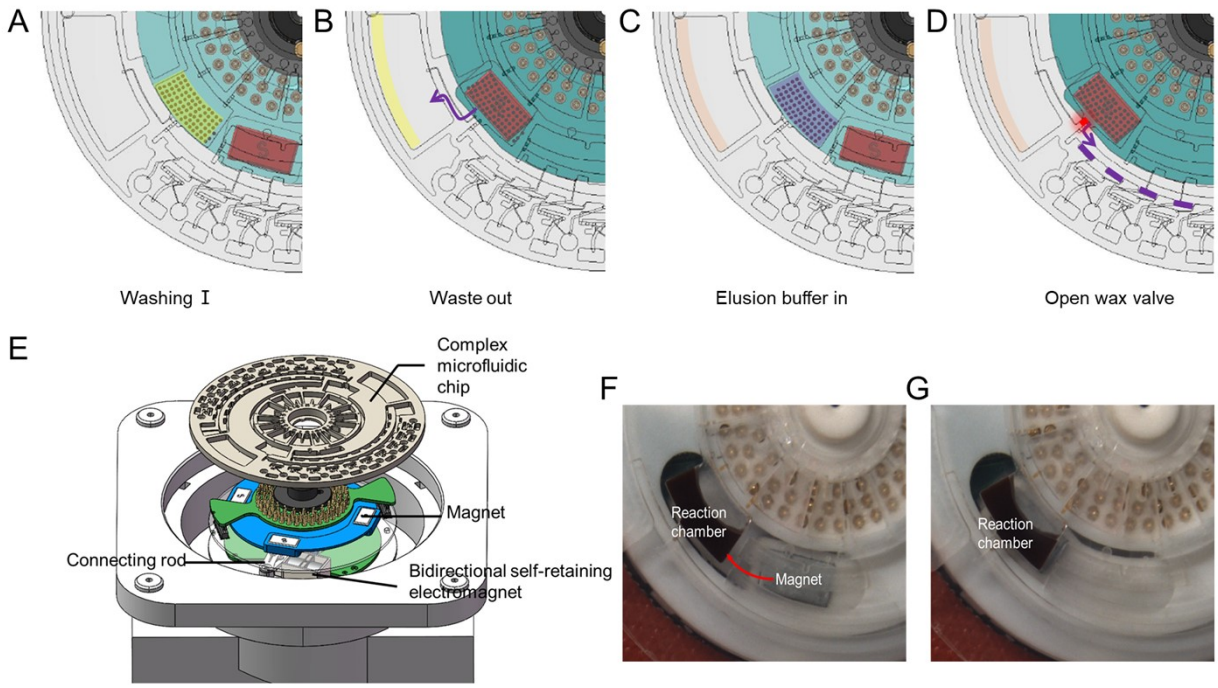

Figure S3. Magnetic switching structure. (**A**) Entrance of Wash buffer I in the reaction chamber while the magnet was away from the reaction chamber. (**B**) Removal of the liquid in the reaction chamber while the magnet was located directly below the reaction chamber. (**C**) Entrance of the elution buffer in the reaction chamber. The liquid in the reaction chamber was removed after 3 min. (**D**) Opening of the paraffin wax valve, located downstream of the reaction chamber. Then, the template flowed into the dosing chamber of the spiral channel while the magnet was below the reaction chamber. (**E**) Design of the magnetic switching structure. (**F**) Image of the nonmagnetic state. The magnet is away from the reaction chamber. (**G**) Image of the magnetic state. The magnet is below the reaction chamber.

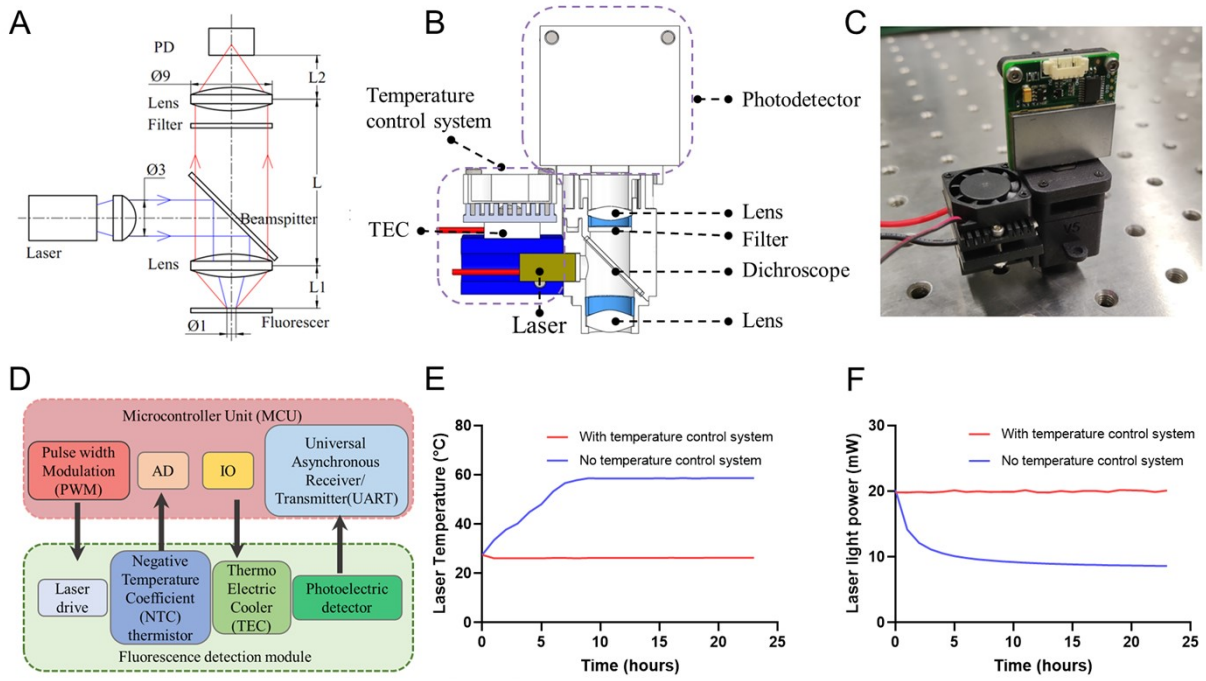

Figure S4. Design of the fluorescence detection module. (**A**) Optical path design. (**B**) Design of the optical detection module. (**C**) Image of the optical structure. (**D**) Hardware system framework of the fluorescence detection module. (**E**) Stability of the semiconductor laser temperature of the optical modules with the temperature control system. (**F**) Stability of the laser power of the optical modules with the temperature control system.

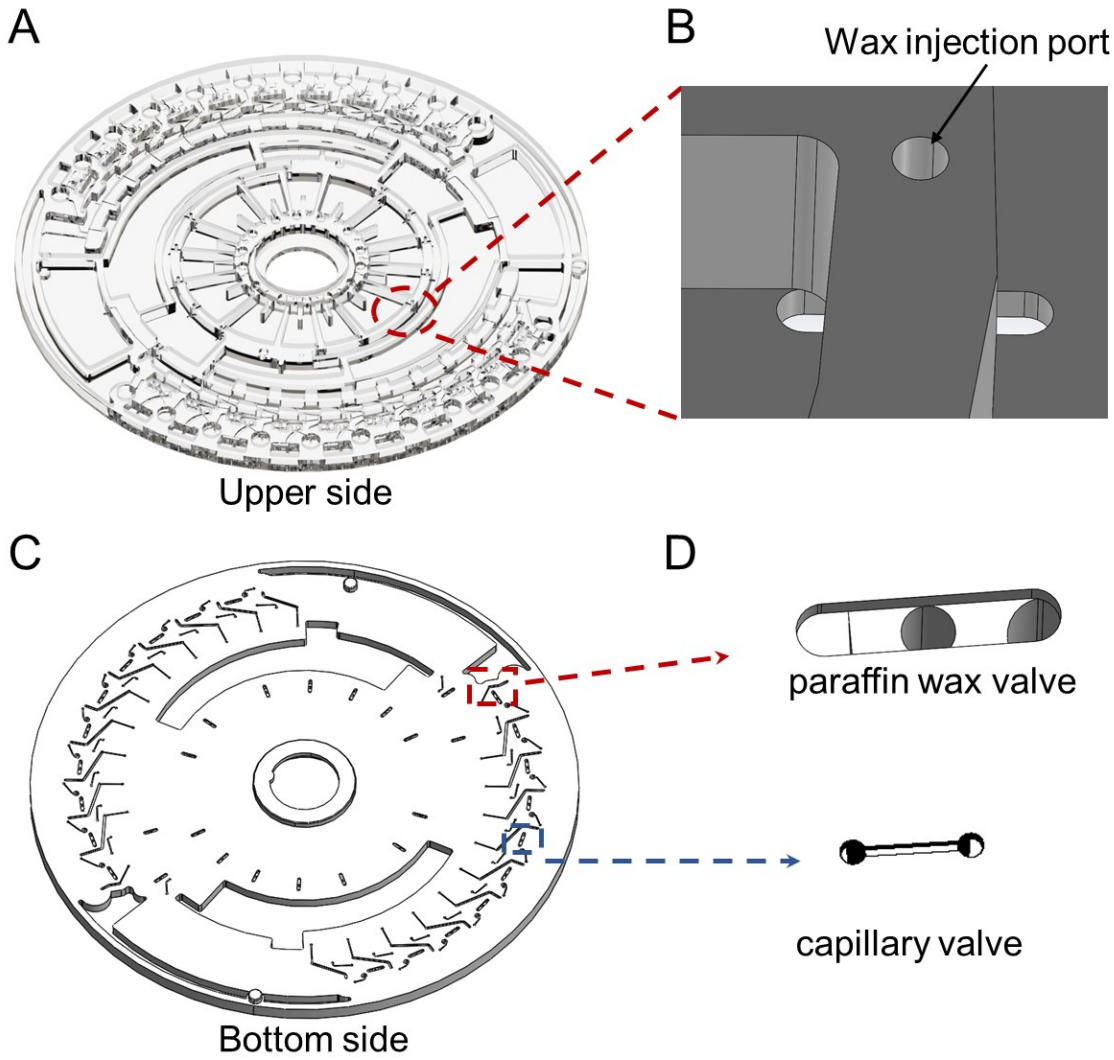

Figure S5. Double side of the microfluidic chip. (**A**) Schematic diagram of the centrifugal microfluidic chip (front view); (**B**) Schematic diagram of the paraffin wax valves (front view); (**C**) Schematic diagram of the centrifugal microfluidic chip (back view); (**D**) Schematic diagram of the paraffin wax valve and capillary valve (back view).

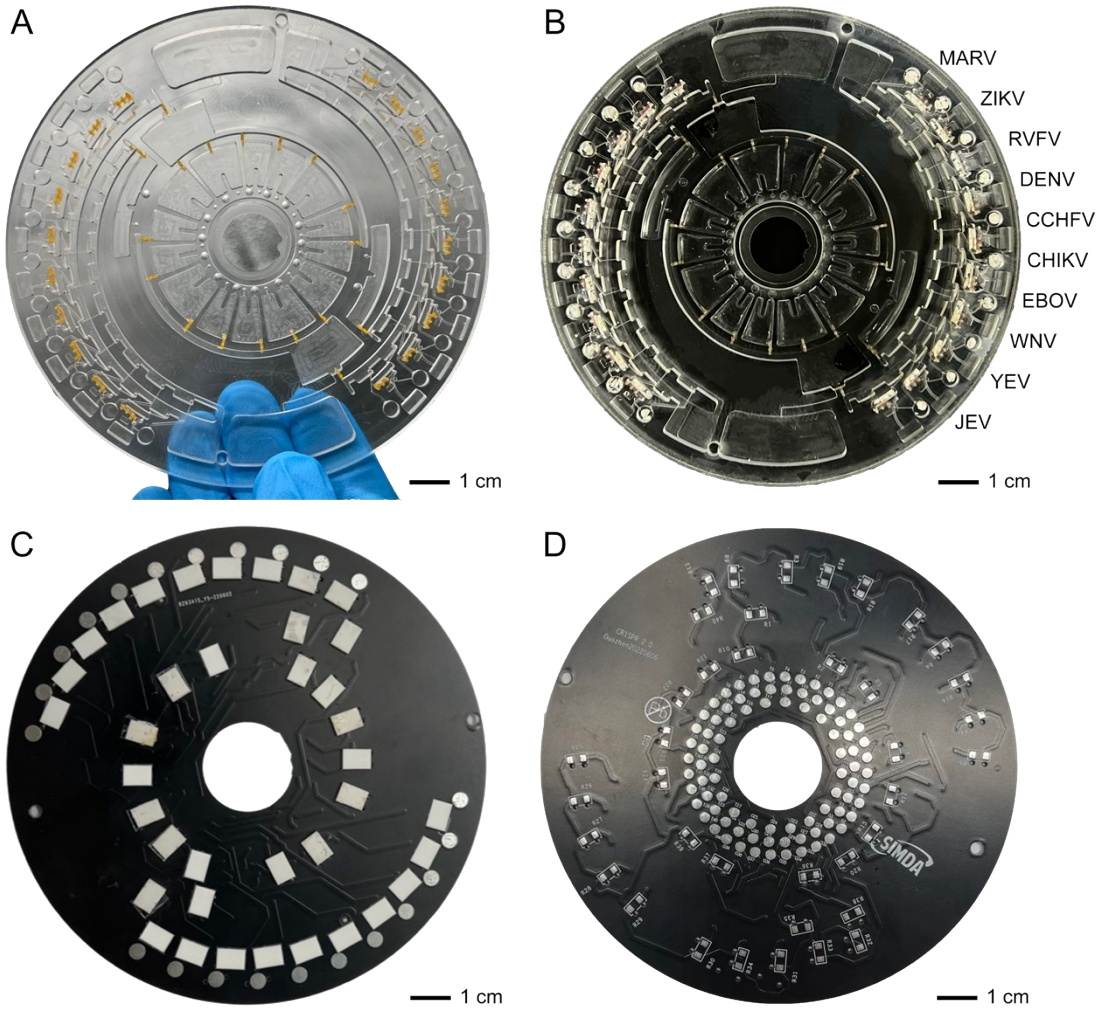

Figure S6. Photograph of the chip and PCB. (**A**) Photograph of the microchannel layer with a paraffin wax valve. (**B**) Photograph of the POCMT chip preloaded with reagents. (**C**) Front view of the valve heating PCB layer. (**D**) Back view of the valve heating PCB layer.

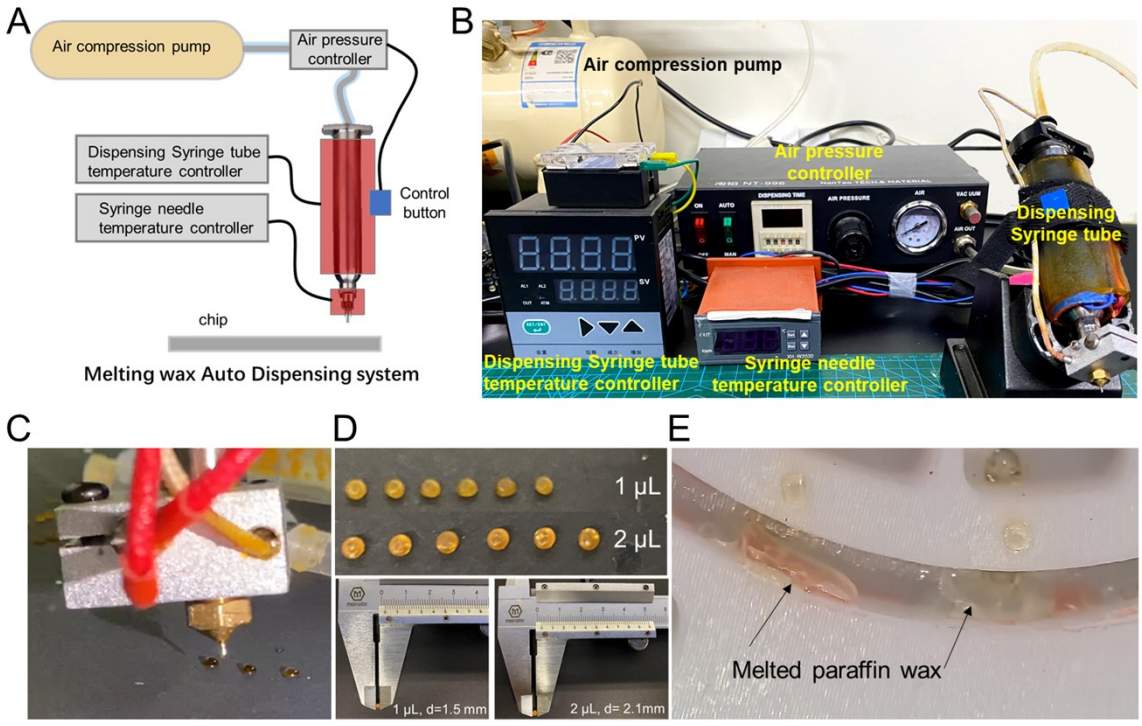

Figure S7. Melting wax auto dispensing system. (**A**) Abridged general view of the equipment for making the paraffin wax valves. (**B**) Image of the equipment for making the paraffin wax valves. (**C**) Image of the paraffin wax. (**D**) Measurement of 1 μL and 2 μL of paraffin wax; (**E**) The final state of the wax on the chip.

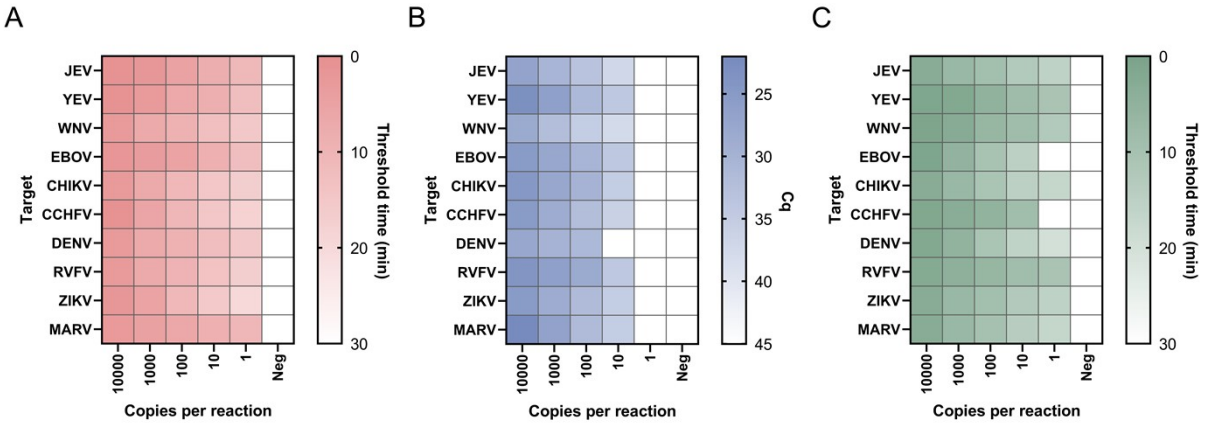

Figure S8. Comparison of the analytical sensitivities of the POCMT system, laboratory-based molecular assay, and traditional CRISPR–Cas-based assay. (**A**) Detection of ten serially diluted pathogen plasmids via the POCMT system. (**B**) Detection of ten serially diluted pathogen plasmids via the laboratory-based molecular assay. The quantification cycle (Cq) values derived from the reverse transcription polymerase chain reaction (RT–PCR) detection systems are shown. (**C**) Detection of ten serially diluted pathogen plasmids via traditional CRISPR–Cas-based assay. The experiments were repeated three times. Neg: negative.

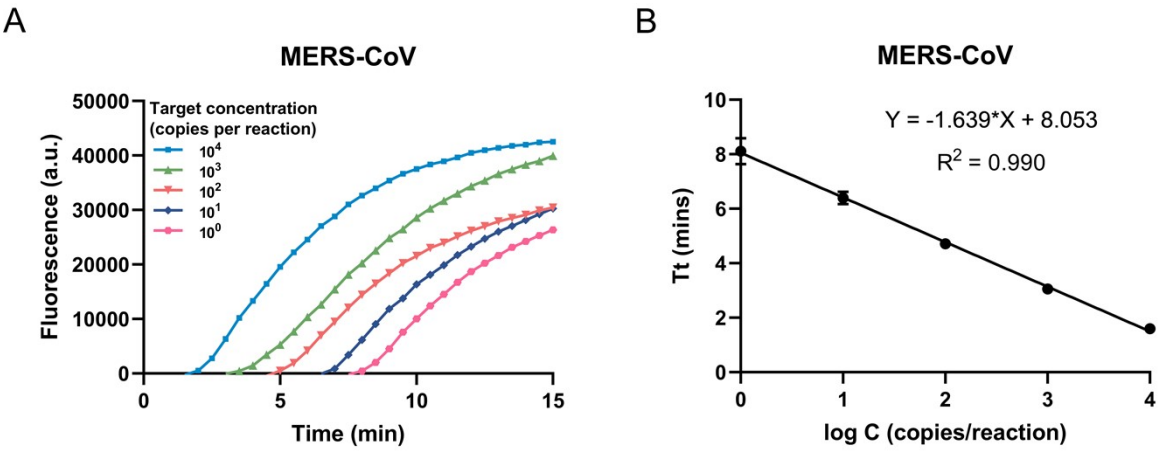

Figure S9. Performance verification in the nasopharyngeal swabs. (**A**) Sensitivity analysis targeting MERS-CoV. (**B**) Relationship between the threshold time to the fluorescence values and logarithmic values of the plasmid concentration for MERS-CoV. The experiments were repeated five times. The error bars represent standard deviations.

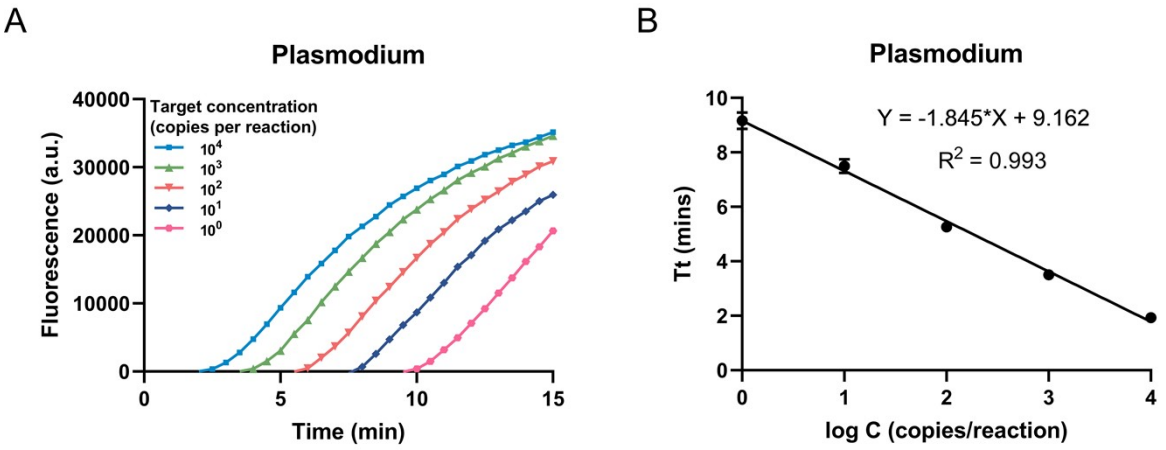

Figure S10. Performance verification in whole blood. (**A**) Sensitive analysis targeting Plasmodium. (**B**) Relationship between the threshold time to the fluorescence values and logarithmic values of the plasmid concentration for Plasmodium. The experiments were repeated five times. The error bars represent standard deviations.

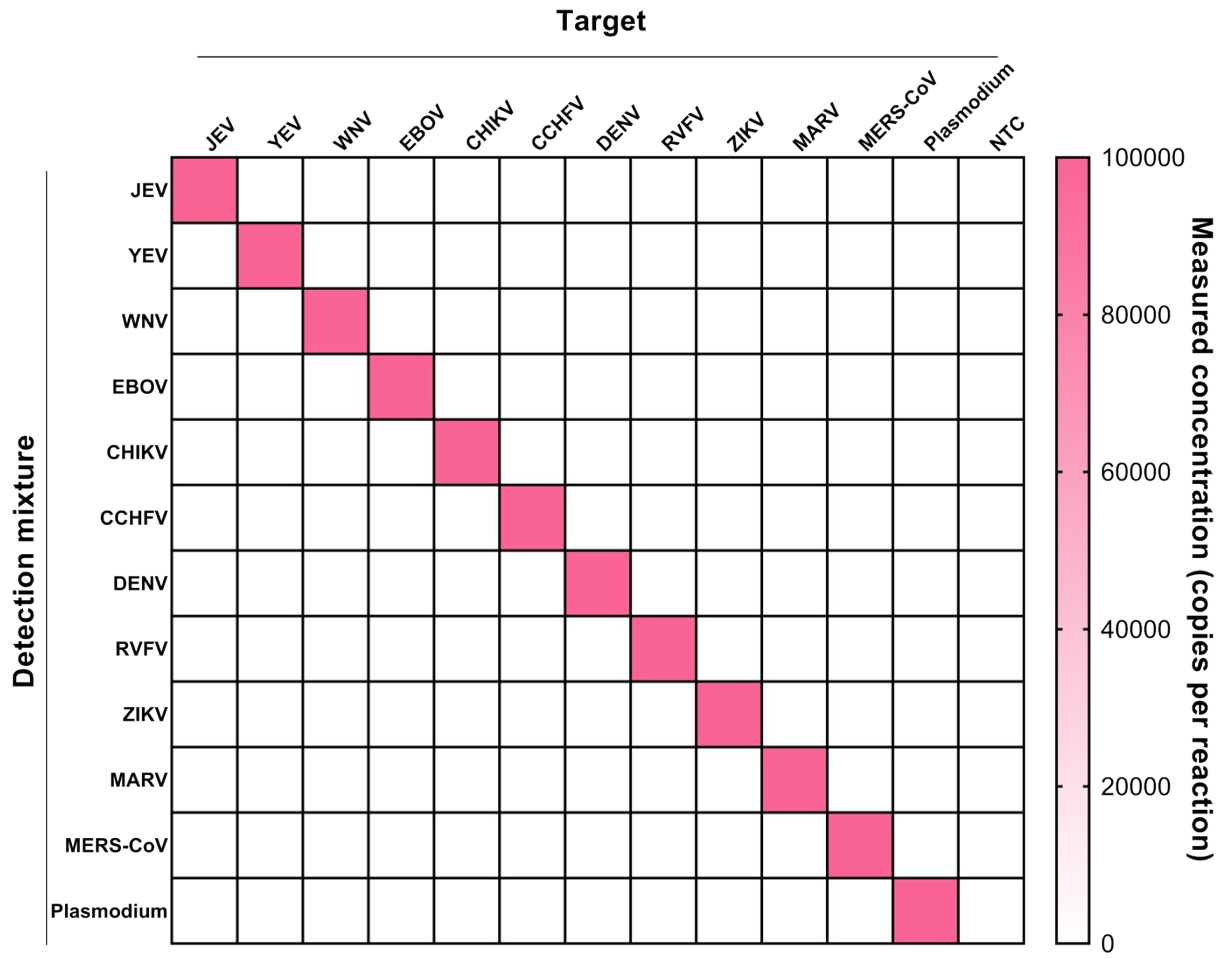

Figure S11. Validation of the analytical specificity by discriminating JEV, YEV, WNV, EBOV, CHIKV, CCHFV, DENV, RVFV, ZIKV, MARV, MERS-CoV and Plasmodium at 10^6 RNA copies per reaction using the POCMT assay. (red zones: positive; blank zones: negative).

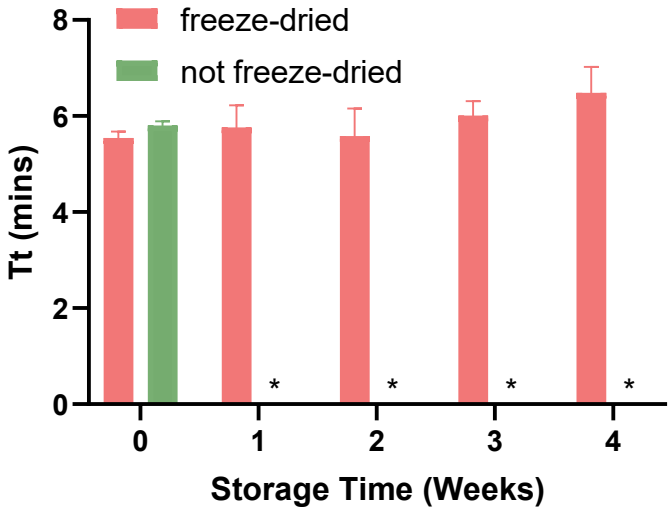

Figure S12. Detection result of the freeze-dried and not freeze-dried reagents within chip storage for 28 days at room temperature. *: The fluorescence signal is not detected.

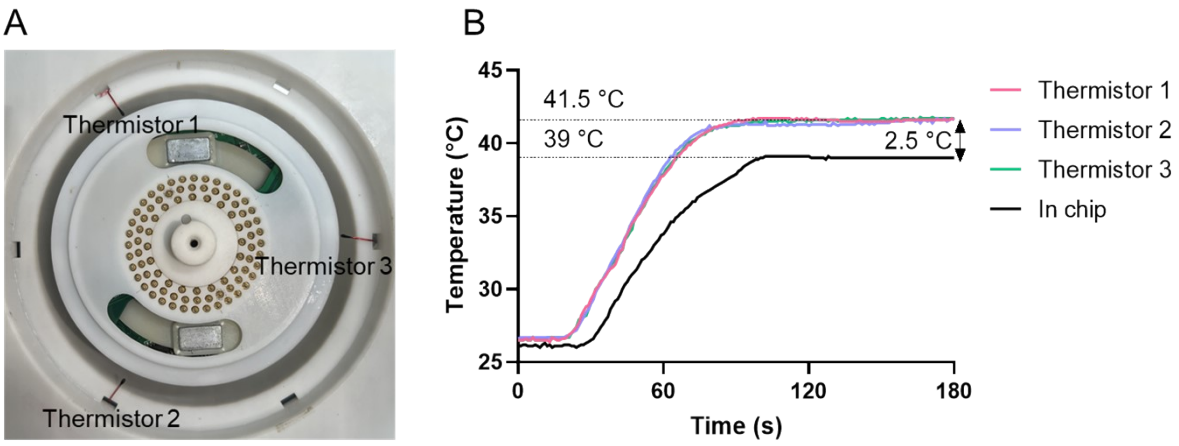

Figure S13. The temperature sampling for the air heating unit. (**A**) The locations of the three thermistors. (**B**) Temperature curves of chip and three thermistors under PID control.

Table S1. Nucleotide sequences of the primers and probes used in this study.

Virus	Gene	Primer/probe	Sequence (5'–3')	Product (base pair)
JEV	M, E	JEV-F	ATCCTYCTGCTGTTGGTCGCTCCGGCTTA	170
		JEV-R	TAATACGACTCACTATAGGGATCATRCGGACRTCYAATGTTGGTTTGTCG	
		JEV- crRNA	TAATACGACTCACTATAGGGGAUUUAGACUACCCCAAAAACGAAGGGGAC UAAAACCAAUCGUGACUUCAUAGAAGGAGCCAGU	
YEV	5'UTR	YEV-F	AAATCCTGKGTGCTAATTGAGGTGYATTGG	119
		YEV-R	TAATACGACTCACTATAGGGACATDWTCTGGTCARTTCTCTGCTAATCGC	
		YEV-crRNA	TAATACGACTCACTATAGGGGAUUUAGACUACCCCAAAAACGAAGGGGAC UAAAACCAAAUCGAGUUGCUAGGCAAUAAACACA	
WNV	prM	WNV-F	CACAGATGTCATCACGATTCCAACAGCTGC	134
		WNV-R	TAATACGACTCACTATAGGGCTTCTGGATCATTACCAGCCGACAGCACTG	
		WNV-crRNA	TAATACGACTCACTATAGGGGAUUUAGACUACCCCAAAAACGAAGGGGAC UAAAACGGAUACAUGUGCGAUGAUACUAUCACUU	
EBOV	NP	EBOV-F	GACGACAATCCTGGCCATCAAGATGATGATCC	169
		EBOV-R	TAATACGACTCACTATAGGGCGTCCTCGTCTAGATCGAATAGGACCAAGTC	
		EBOV-crRNA	TAATACGACTCACTATAGGGGAUUUAGACUACCCCAAAAACGAAGGGGAC UAAAACGGUGGUUGAUCCCGAUGAUGGAAGCUAC	
CHIKV	NSP1	CHIKV-F	TCACAYCRAATGACCAYGCTA ATGCTAGAGC	136
		CHIKV-R	TAATACGACTCACTATAGGGTTCCTRTCCGACATCATCCTCCTTGCTGGYGC	

		CHIKV-crRNA	TAATACGACTCACTATAGGGGAUUUAGACUACCCCAAAAACGAAGGGGAC UAAAACGCUAAUGCUAGAGCGUUCUCGCAUCUAG	
CCHFV	NP	CCHFV-F	AGAAACACGTGCCGCTTACGCCCACAGTGTT	150
		CCHFV-R	TAATACGACTCACTATAGGGTAGGAGTTTGTGAAAGTGTCCATAAGTCCAT T	
		CCHFV-crRNA	TAATACGACTCACTATAGGGGAUUUAGACUACCCCAAAAACGAAGGGGAC UAAAACUGAGUGCUAGCAGAAUGGAGAAUAAAAU	
DENV	IncRNA	DENV-F	AGCATATTGACGCTGGGARAGACCAGAGAT	104
		DENV-R	TAATACGACTCACTATAGGGGAACCTGTTGRWTCAACARCACCAWTCCAT	
		DENV-crRNA	TAATACGACTCACTATAGGGGAUUUAGACUACCCCAAAAACGAAGGGGAC UAAAACGCACAGAACGCCAGAAAAUGGAAUGGUG	
RVFV	NC	RVFV-F	CATTTTCATCATCATCCTCCKGGGCTTRTTG	108
		RVFV-R	TAATACGACTCACTATAGGGGARCTCYTAAAGCAGTATGGTGGGGCTGACT	
		RVFV-crRNA	TAATACGACTCACTATAGGGGAUUUAGACUACCCCAAAAACGAAGGGGAC UAAAACCGAGUCAGAGCCAGAACAAUCAUUUUCU	
ZIKV	NS5	ZIKV-F	CCACAGAAGRGACCTYCGACTGATGGCYAATGC	160
		ZIKV-R	TAATACGACTCACTATAGGGCTCCTCAATCCACACTCTRTTCCACACCAYR AG	
		ZIKV-crRNA	TAATACGACTCACTATAGGGGAUUUAGACUACCCCAAAAACGAAGGGGAC UAAAACTGACTGGGTTCCAACTGGGAGAACTACC	
MARV	NP	MARV-F	CATGAACATCAGGAAATTCAAGCTATTGCMGARG	136
		MARV-R	TAATACGACTCACTATAGGGCTAATTTTTCTCGTTTCTGGCTGAGGACGGC	

		MARV-crRNA	TAATACGACTCACTATAGGGGAUUUAGACUACCCCAAAAACGAAGGGGAC UAAAACGGAAGATATTAGAACAGTTCCACCTTCA	
MERS-CoV	NC	MERS-CoV-F	AACTTCCACATTGAGGGGACTGGAGGCAA	111
		MERS-CoV-R	TAATACGACTCACTATAGGGAGAGTTTCCTGATCTTGAACCTTGTGAACT	
		MERS-CoV-crRNA	TAATACGACTCACTATAGGGGAUUUAGACUACCCCAAAAACGAAGGGGAC UAAAACUCAAGAGCCUCUAGCGUAAGCAGAAACU	
Plasmodium	PBANKA	Plasmodium-F	CCATTAATCAAGAACGAAAGTTAAGGGAGTG	183
		Plasmodium-R	TAATACGACTCACTATAGGGCTCGCCCCAGAACCCAAAGACTTTGATTTCT C	
		Plasmodium- crRNA	TAATACGACTCACTATAGGGGAUUUAGACUACCCCAAAAACGAAGGGGAC UAAAACGGAATTCTTAGATTGCTTCCTTCAGTAC	

Table S2. Comparison of the DENV detection results in the traditional CRISPR–Cas-based assay and microfluidic platform for the 45 clinical samples.

Microfluidic platform	Traditional CRISPR–Cas-based assay		Total
	Positive	Negative	
Positive	24	0	24
Negative	0	21	21
Total	24	21	45

Movie 1.
Reagent release controlled by addressable active thermally-triggered wax valves

Movie 2.
Switching of magnetic states

Movie 3.
Demonstration of flow control and process on the chip

Movie 4.
Melting wax auto dispensing system

Movie 5
Demonstration of the heating process